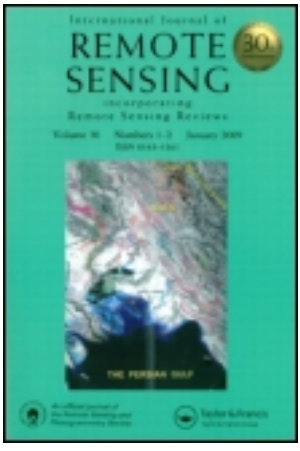

International Journal of Remote Sensing
Publication details, including instructions for authors and subscription information:
http://www.tandfonline.com/loi/tres20

Application of the dense medium radiative transfer theory for calculating microwave emissivities of different sea ice types

K. Schmidt & J. Wauer

Version of record first published: 25 Nov 2010.

To cite this article: K. Schmidt & J. Wauer (1999): Application of the dense medium radiative transfer theory for calculating microwave emissivities of different sea ice types, International Journal of Remote Sensing, 20:15-16, 3165-3182

To link to this article: http://dx.doi.org/10.1080/014311699211688

INT. J. REMOTE SENSING, 1999, VOL. 20, NO. 15 & 16, 3165–3182

Application of the dense medium radiative transfer theory for calculating microwave emissivities of different sea ice types

K. SCHMIDT and J. WAUER

German Aerospace Centre, German Remote Sensing Data Centre, Kalkhorstweg 53, D-17235 Neustrelitz, Germany; e-mail: schmidt@nz.dlr.de

(*Received 8 February 1998; in final form 1 December 1998*)

Abstract. The dense medium radiative transfer theory (DMRT) was used to calculate microwave emissivities of different undeformed sea ice types in the Arctic and Antarctic. The computed results were compared with measurements. More often taken for describing snow, we show that the DMRT can be applied to both sea ice and snow cover. While doing so the choice of appropriate parameters needed in the DMRT is discussed. As a result a multi-layered, uniform model for a variety of sea ice types including snow cover is obtained.

1. Introduction

Sea ice observations play an important role in climate and ice physics studies as well as in ship operations. In these observations the primary interest is focused on ice concentration, areal coverage of ice versus open water, ice type including old, first-year and thin ice, ice depth, topography and accumulation rate, ice motion and snow cover. A variety of existing and planned remote sensing systems provide the possibility to gain data on these properties (for a review see, e.g., Carsey 1992a, b). Among them, microwave radiometers and Synthetic Aperture Radar (SAR) systems are especially suited to derive information about sea ice composition and structure because the received signals are influenced not only by surface but also by characteristic volume scattering processes in the ice. In interpreting the signatures, physically based models are needed. Different microwave sea ice models are reviewed in Winebrenner *et al.* (1992a). Since snow and sea ice represent dense media (the scattering particles such as ice grains, brine pockets or air bubbles can occupy up to 50% of the total volume) any volume scattering model should account for dense media effects.

One volume scattering model that takes into account dense media effects is given by the dense medium radiative transfer theory (DMRT; Tsang and Ishimaru 1987, Tsang 1987). It represents a model that describes the propagation and scattering of electromagnetic waves in a system consisting of discrete Rayleigh scatterers embedded in a homogeneous background medium. Starting from the clear picture of discrete, regularly shaped particles, a set of exact multiple scattering equations based on Maxwell's equations can be derived (Tsang *et al.* 1985). Ensemble averages of the

International Journal of Remote Sensing
ISSN 0143-1161 print/ISSN 1366-5901 online
http://www.tandf.co.uk/JNLS/res.htm
http://www.taylorandfrancis.com/JNLS/res.htm

multiple scattering equations led to Dyson's equation for the coherent field and to the Bethe-Salpeter equation for the second moment of the incoherent intensity. The DMRT results from the quasi-crystalline approximation with coherent potential (QCA-CP) of Dyson's equation and the ladder approximation of the Bethe-Salpeter equation. Note that both approximations are consistent in energy conservation. The DMRT takes into account correlations of the particle positions in the case where the particles occupy an appreciable fraction of the total volume of the system. These correlations are approximated to be always interactions between two particles only and are modelled by the Percus-Yevick pair distribution function for hard spheres. One important advantage of the DMRT is that, while the extinction coefficient κ_e and albedo $\tilde{\omega}$ depend on the particle correlation, it takes the form of the ordinary radiative transfer equation developed by Chandrasekhar (1960). In this way all known methods of the classical radiative transfer theory can be used for its solution. Originally developed for single sized spheres, Tsang and co-workers (Tsang *et al.* 1990, Tsang 1992) have generalized the DMRT to treat Rayleigh spheres of multiple sizes and permittivities.

So far, the DMRT has been mainly applied to snow (e.g. Tsang 1987, Ding 1989, Wen *et al.* 1990, Tsang *et al.* 1990, Tsang 1992, Tsang *et al.* 1992, West *et al.* 1993, Jin 1993, Ding *et al.* 1996, Jin 1997a, b) and firn (e.g. West *et al.* 1994, Winebrenner *et al.* 1997). In these investigations it could be shown that it represents an appropriate method for describing the electromagnetic properties of these media. To the best of our knowledge, applications to sea ice are relatively scarce and limited to multi-year ice (Winebrenner *et al.* 1989, Winebrenner *et al.* 1992a, b, Dierking 1992). In this paper, we therefore want to focus on different undeformed sea ice types in the Arctic and Antarctic, and calculate their microwave emissivities by means of the DMRT. The aim of our investigations is twofold. First, we want to demonstrate the capabilities of the DMRT to treat various ice types including snow cover. Second, a gap is still open concerning the ice modelling in Winebrenner *et al.* (1992a) by means of the DMRT. It was the hope of the authors that future calculations using DMRT could help in understanding the effect of scattering on emission especially from melt ponds. In this paper we present results for the sea ice examples given there.

2. Model description

The ice and the overlying snow, if present, were modelled as a multi-layered system with planar interfaces and topped by a planar surface. The subdivision into different layers was based on depth-dependent snow and ice properties such as structural and physical properties (density ρ, temperature T, salinity S). Corresponding values and profiles were taken from ice core analyses and snow and ice thickness measurements given in the literature. It was assumed that the snow and ice parameters are constant within each layer. For describing this system the DMRT generalized to Rayleigh spheres of multiple sizes and permittivities was used. This allowed us to consider different scatterer types in each layer. Within the framework of the DMRT, the passive vector radiative transfer was governed by the following equation (e.g Chandrasekhar 1960, Tsang 1987, Tsang *et al.* 1990, Tsang 1992).

$$\mu \frac{\mathrm{d}\bar{I}(\mu,\tau)}{\mathrm{d}\tau} = \bar{I}(\mu) - \frac{\tilde{\omega}}{2}\int_{-1}^{1} \mathrm{d}\mu' \,\bar{\bar{P}}(\mu,\mu')\,\bar{I}(\mu',\tau) - (1-\tilde{\omega})\,\bar{B}(T) \qquad (1)$$

Here, $\bar{I}=(I_v, I_h, U, V)$ denotes the Stokes vector, $\bar{\bar{P}}$ the Rayleigh phase matrix, and $\bar{B}(T)$ the Planck function written as a vector. The variable μ is defined by $\mu=\cos\theta$. $\tau=-z\cdot\kappa_e$ designates the optical thickness at the height z. Expressions for the extinction coefficient κ_e and the albedo $\tilde{\omega}$ of a dense system with Rayleigh spheres of multiple sizes and permittivities can be found, for instance, in Ding (1989), Tsang *et al.* (1990) and Tsang (1992). In the following, let L be the number of species and let a_l, f_l, ε_l, and $k_l=\omega\sqrt{\mu_0\varepsilon_l}$ be the radius, the fractional volume, the permittivity, and the wavenumber, respectively, of the species $l=1, \ldots, L$. Then, it holds

$$\kappa_e = 2\cdot Im(K_{eff}) \tag{2}$$

$$\tilde{\omega}=\frac{2|K_{eff}|^4}{\kappa_e|D|^2}\sum_{l=1}^{L} f_l y_l\cdot\left[a_l^3 y_l^* + \sum_{j=1}^{L} 8\pi^3 n_j a_j^3 y_j^* H_{jl}(p=0)\right] \tag{3}$$

$$y_l=\frac{k_l^2-k_{bg}^2}{3K_{eff}^2+(k_l^2-k_{bg}^2)} \tag{4}$$

$$D=1-\sum_{l=1}^{L} f_l y_l. \tag{5}$$

In the above equations, k_{bg} denotes the wavenumber of the background with the permittivity ε_{bg} in which the scatterers are embedded. $n_l=3f_l/(4\pi a_l^3)$ is the number of particles of the species l per unit volume, and the function $H_{jl}(p)$ is the Fourier transform of the total correlation function describing the pair interaction of the scatterers. Within the framework of the DMRT, the Percus-Yevick total correlation function for hard spheres was used. Corresponding expressions and computational details for a mixture of multiple species are given in, e.g., Ding and Tsang (1988), Ding and Tsang (1989), Ding (1989), and Ding *et al.* (1992). The quantity $K_{eff}=\omega\sqrt{\mu_0\varepsilon_{eff}}$ designates the effective propagation constant which characterizes the propagation of a coherent wave through a medium with an effective permittivity ε_{eff}. K_{eff} results from the solution of the dispersion relation for QCA-CP. A closed form expression can be derived in the low-frequency limit when the particles are smaller than the wavelength (Ding and Tsang 1988, Ding and Tsang 1989, Ding 1989).

$$K_{eff}^2=k_{bg}^2+\frac{3K_{eff}^2}{D}\sum_{l=1}^{L} f_l y_l \times\left[1+i\frac{2K_{eff}^3}{3D}\left(a_l^3 y_l+\sum_{j=1}^{L} 8\pi^3 n_j a_j^3 y_j H_{jl}(p=0)\right)\right] \tag{6}$$

The radiative transfer equation (1) is solved for the multi-layered system with constant parameters within each layer by means of the discrete-ordinate method (Stamnes *et al.* 1988). This method uses a discretization with respect to μ so that the integro-differential equation (1) is approximated by a coupled system of linear differential equations with constant coefficients. The general solution for each layer can be found by a solution of an eigenvalue problem. Inserting the general solutions of all layers into the boundary conditions of the Stokes vectors at the planar interfaces, which are, for instance, given in Jin (1993), yields a linear equation system

for determining the integration constants. Note that the lowest layer is treated as an infinite half-space. From the known intensities I_β, $\beta=(v,h)$, the emissivity e_β is readily obtained using the Rayleigh-Jean's approximation.

$$e_\beta = \frac{I_\beta \lambda^2}{K_B T} \tag{7}$$

Here, K_B denotes Boltzmann's constant and λ is the given wavelength. For comparison purposes with the effective emissivities of Winebrenner *et al.* (1992a) and Grenfell *et al.* (1994), the snow–ice interface and ice surface temperature, respectively, is taken in equation (7) depending on whether a snow cover is present or not.

It is seen from the above equations that the application of the DMRT requires the specification of the background and the scatterers in each layer including the parameters particle radii a_l, fractional volumes f_l of the particles, scatterer (ε_l) and background (ε_{bg}) permittivities. Table 1 summarizes the procedure by which we determine the volume fractions and permittivities. In general, we considered two basic types of media: snow and sea ice. The host medium in snow is assumed to be air with the permittivity ε_0. Ice grains embedded in the air act as scatterers. The ice permittivity was calculated by a model for fresh-water ice developed in (Mätzler and Wegmüller 1987). In our calculations, however, we neglected saline impurities so that pure ice is assumed. The fractional volume of ice was computed by means of the simple formula (Ulaby *et al.* 1986)

$$f_{ice} = \frac{\rho_{snow}}{0.916} \tag{8}$$

where ρ_{snow} is the dry snow density in g cm^{-3}. If only ice grains, as described above, are used as scatterers, dry snow is modelled. Wet snow is obtained by adding water inclusions. The permittivity of water is computed taking the Debye expression of Klein and Swift (1977). The water volume fraction can be freely chosen. In this way we are able to switch between dry and wet snow.

Pure ice is considered to be the background medium in sea ice. As in the case of ice grains in snow, its permittivity was calculated by the expressions of Mätzler and Wegmüller (1987), omitting saline impurities. Air bubbles and brine pockets represent scatterers in sea ice. The brine permittivity was taken from Stogryn and Desargant (1985). An approximate expression for the air volume fraction can be found in Cox

Table 1. Specification of the background and the scatterers in snow and sea ice including parameters needed in applying the DMRT. CW'83 (Cox and Weeks 1983), KS'77 (Klein and Swift 1977), MW'87 (Mätzler and Wegmüller 1987), SD'85 (Stogryn and Desargant 1985), UMF'86 (Ulaby *et al.* 1986).

Type	Background	ε_{bg}	Scatterers	ε_l	f_l
snow	air	ε_0	ice grains water inclusions	MW'87 KS'77	UMF'86 free parameter
sea ice	pure ice	MW'87	air bubbles brine pockets	ε_0 SD'85	CW'83 UMF'86/CW'83

and Weeks (1983). For evaluating the brine volume fraction we used, e.g., Ulaby *et al.* (1986) and Fung (1994).

$$f_{\mathrm{brine}} = \frac{S_{\mathrm{ice}} \cdot \rho_{\mathrm{ice}}}{S_{\mathrm{brine}} \cdot \rho_{\mathrm{brine}}} \tag{9}$$

Here, S_{ice} and S_{brine} are the sea ice and brine salinity, respectively. The latter quantity is related to the temperature by some empirical expressions (Poe *et al.* 1972, see also Ulaby *et al.* 1986, Fung 1994) which were taken in our calculations. ρ_{ice} and ρ_{brine} (in $\mathrm{g\,cm^{-3}}$) denote the pure ice and brine density, respectively, and are related to the temperature T (in °C) by the following equations (Cox and Weeks 1983):

$$\rho_{\mathrm{ice}} = 0.917 - 1.403 \times 10^{-4} \times T \tag{10}$$

$$\rho_{\mathrm{brine}} = 1 + 0.0008 \times S_{\mathrm{brine}}(T) \tag{11}$$

In all computations, the particle radii were treated as free parameters in order to fit the calculated emissivities to known values from the literature. As a first test for the chosen parameters, the calculated effective permittivities $\varepsilon_{\mathrm{eff}} = K_{\mathrm{eff}}^2/(\omega^2 \mu_0)$ based on equation (6) were compared with values from the literature. In varying the particle radii, the fulfilment of the Rayleigh approximation (small $k_{\mathrm{bg}} \cdot a_l$) has to be ensured. As we will see later, this can become, however, crucial for higher frequencies. Additionally, the variation is performed within realistic particle dimensions taken from observations or measurements. Note that by changing, e.g., the different radii and salinity, various ice types such as young ice without air bubbles or old, desalinated ice can be modelled from our basic type 'sea ice'.

On the basis of the chosen parameters discussed above, the dielectric and radiative properties of the medium in each layer were calculated within the DMRT. In this way, a uniform and self-consistent description for various snow and sea ice types was given. In the following section we present some results of our investigations.

3. Numerical examples

3.1. *CRRELEX thin grey ice*

First, we calculated the emissivities of a thin, snow-free grey ice sheet grown as part of the 1998 CRRELEX experiment at the Cold Regions Research and Engineering Laboratory in Hanover, New Hampshire. A detailed description of this ice and its modelling is given in Winebrenner *et al.* (1992a). Note that no results for this ice type based on the DMRT are provided by Winebrenner *et al.* (1992a). Table 2 shows the parameters used in our computations. Here, d denotes the thickness of the corresponding layer. The temperature and salinity profile were taken from measurements on the morning of 15 January 1988, and the sea ice density was assumed to be $0.91\,\mathrm{g\,cm^{-3}}$ in each layer. It should be mentioned that in the physical optics model under the scalar approximation (Winebrenner *et al.* 1992a), an ice density of $0.92\,\mathrm{g\,cm^{-3}}$ is assumed. Brine pockets with radii of about 0.1 mm were considered to be the scatterers. The dense medium theory-integral equation method (Winebrenner *et al.* 1992a) also uses spherical brine pockets with a radius of 0.1 mm. This value is typical for young and first-year ice (Perovich and Gow 1996).

In figure 1, the calculated and observed emissivities for different frequencies at an observation angle of 50° are plotted. Here and in the following examples, calculations were performed at 6.7, 10, 18.7, 37 and 90 GHz. In the case of the vertical (v) polarization, good agreement is obtained. The horizontally (h) polarized emissivities

Table 2. Parameters used in the emissivity calculations for the CRRELEX grey ice sheet. By taking equation (9), the computed brine volume fractions are 0.101 for the first ice layer, and 0.053, 0.076, 0.082, 0.082, 0.076, 0.087 and 0.119 for the following ice layers.

Medium	d (cm)	T (K)	ρ (g cm^{-3})	S (‰)	a_{brine} (mm)
sea ice	1	262.8	0.91	17.8	0.15
sea ice	1	264.4	0.91	8.5	0.1
sea ice	1	266.3	0.91	10.0	0.1
sea ice	1	267.6	0.91	9.0	0.1
sea ice	1	268.4	0.91	7.8	0.1
sea ice	1	269.1	0.91	6.2	0.1
sea ice	1	269.9	0.91	5.8	0.1
sea ice	1	270.6	0.91	6.3	0.1
sea water	∞	272.1	1.0	24.0	0

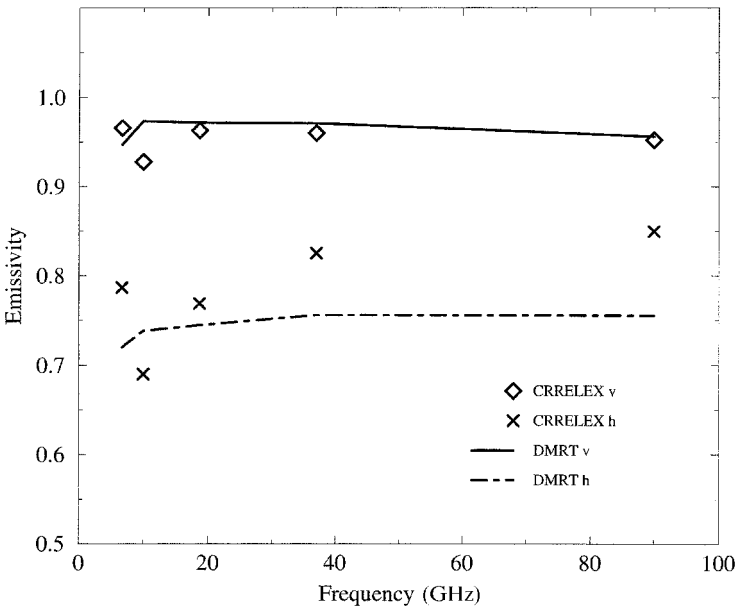

Figure 1. Comparison of observations made during the CRRELEX experiment with emissivities computed using the DMRT for the grey ice sheet. Emissivity versus frequency at an observation angle of 50°. The parameters for the DMRT calculations are given in table 2.

are too low, except at 10 GHz where a minimum in the experimental data occurs which is assumed to be a real feature. We were not able to reproduce this minimum. Changes of the density or brine radii lead to no improvements. Figure 2 shows the emissivities as a function of the observation angle at 18.7 GHz. Good agreement between theory and experiment is obtained.

3.2. *Old ice at DS-7*

Next, we investigated the microwave emission of the ice at the drift station site 7 (DS-7), Arctic Ocean, north of the Barents Sea. Experimental data of this site were acquired from 3 October to 8 October 1988, as part of the CEAREX experiment.

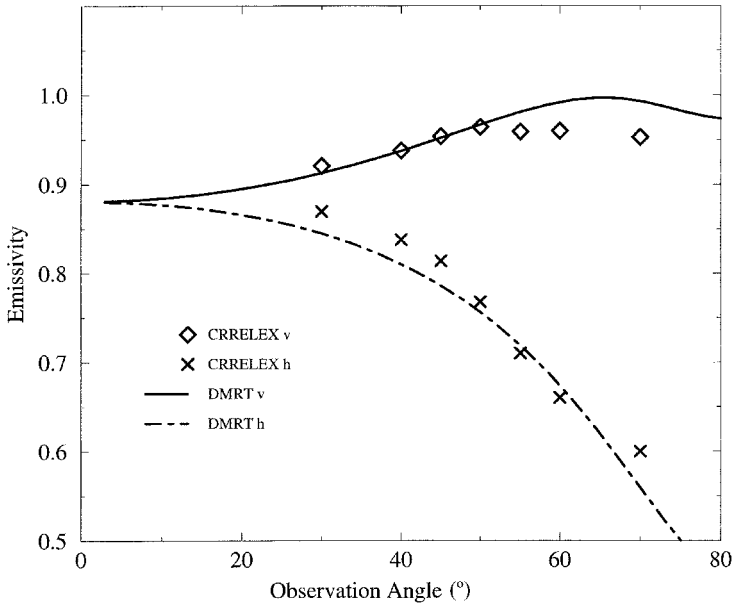

Figure 2. Comparison of observations made during the CRRELEX experiment with emissivities computed using the DMRT for the grey ice sheet. Emissivity versus observation angle at 18.7 GHz. The parameters for the DMRT calculations are given in table 2.

Details about these data, together with computational results from different models, are given in Winebrenner *et al.* (1992a). Note that the DMRT was applied to this ice for calculating the 10 GHz backscattering. Good agreement between observations and computations for both, like- and cross-polarized cross sections, were achieved.

The ice at DS-7 represents cold old ice, the uppermost layers of which consisted of a fragile, geometrically complex matrix of air and ice containing many bubbles and some irregular, interconnected air spaces called voids. This structure especially and the resulting strong scattering made accurate computation difficult. Neither of the two models (many layer strong fluctuation theory and modified radiative transfer; see Winebrenner *et al.* (1992a)) applied to this ice for calculating the emissivities could accurately explain the passive observations.

Table 3 shows the parameters used in our calculations. The density and salinity profile were taken from figures 8–10 in Winebrenner *et al.* (1992a) and from additional explanations in the text. The temperature profile was estimated on the basis of Grenfell's measurements. Our ice grain radius a_{ice} represents the lower limit of the grain dimensions reported. Onstott visually derived mean bubble diameters and characteristic void dimensions, at 2.5 mm and 8 mm, respectively, in the upper, most porous ice layer, and 4 mm and 2 mm, respectively, in the underlying layer. Based on these data, an air bubble radius a_{air} of 2 mm in the upper and of 1.5 mm in the next layer was assumed in our computations. The layer below these two was modelled with $\rho = 0.84\,\mathrm{g\,cm^{-3}}$, $S = 0.05$ (‰), $a_{air} = 0.5$ mm, and $a_{brine} = 0.1$ mm. For simplicity, the brine radius was kept constant in all the following ice layers.

In figure 3, our results for the emissivities versus frequency at an observation angle of 50° are plotted. For both polarizations, the agreement between theory and experiment was good up to 18.7 GHz. However, the calculations predicted too low

Table 3. Parameters used in the emissivity calculations for the ice at DS-7. By taking equation (8), the computed ice volume fraction of the snow layer is 0.109. Based on the model by Cox and Weeks (1983), the calculated air volume fractions for the first three ice layers are 0.502, 0.207 and 0.085. Equation (9) provides for the brine volume fractions 2.9×10^{-4}, 5.9×10^{-4}, 1.8×10^{-3}, 4.4×10^{-3}, 7.7×10^{-3}, 9.2×10^{-3}, 0.013, 0.017 and 0.022, beginning with the third ice layer.

Medium	d (cm)	T (K)	ρ (g cm^{-3})	S (‰)	a_{ice} (mm)	a_{air} (mm)	a_{brine} (mm)
dry snow	10	259.1	0.1	0	0.1	0	0
sea ice	5	263.0	0.457	0	0	2.0	0
sea ice	3.5	263.1	0.728	0	0	1.5	0
sea ice	10.5	263.3	0.84	0.05	0	0.5	0.1
sea ice	9	263.5	0.895	0.1	0	0	0.1
sea ice	8	263.9	0.895	0.3	0	0	0.1
sea ice	17	264.5	0.895	0.7	0	0	0.1
sea ice	14	264.8	0.895	1.2	0	0	0.1
sea ice	10	265.1	0.89	1.4	0	0	0.1
sea ice	10	265.4	0.88	1.9	0	0	0.1
sea ice	5	265.7	0.87	2.4	0	0	0.1
sea ice	58	266.1	0.87	3.0	0	0	0.1
sea water	∞	269.9	1.0	32	0	0	0

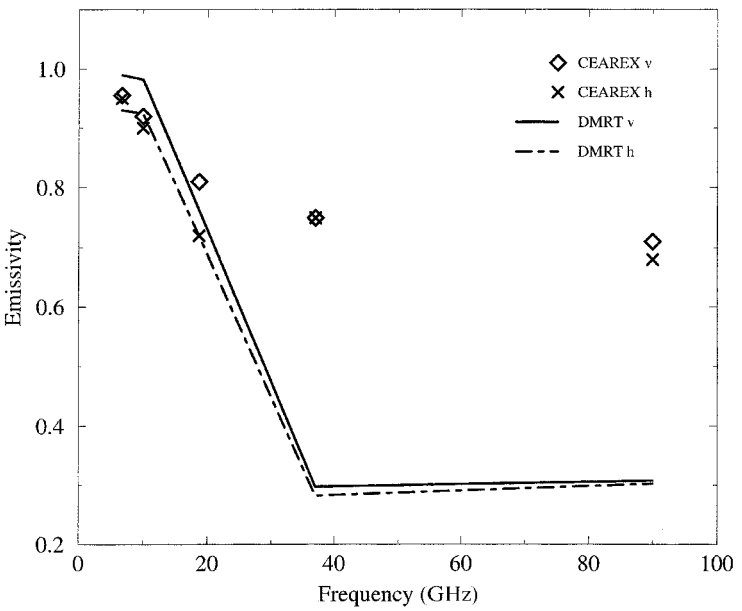

Figure 3. Comparison of observations made during the CEAREX experiment with emissivities computed using the DMRT for the ice at DS-7. Emissivity versus frequency at an observation angle of 50°. The parameters for the DMRT calculations are given in table 3.

emissivities at 37 GHz and 90 GHz. In contrast to this, the many layer strong fluctuation theory and the modified radiative transfer obtained too high emissivities at these frequencies (Winebrenner *et al.* 1992a). A look at the size parameters of the air bubbles reveals the reason for the disagreement at higher frequencies. For instance,

the size parameter of the largest air bubble with $a_{air} = 2.0$ mm was about 6.7 at 90 GHz, 2.8 at 37 GHz, 1.4 at 18.7 GHz, 0.7 at 10 GHz, and 0.5 at 6.7 GHz. Remember that the background permittivity is used to calculate size parameters. One of the basic assumptions in deriving DMRT is the Rayleigh approximation (small $k_{bg} \cdot a_{air}$) which is violated at 37 GHz and 90 GHz. Its usage at 18.7 GHz seems to be, at least, questionable. This means that, the DMRT in its present form is not applicable to such large particles. Rayleigh scattering increases rapidly with increasing size parameter, and its application to particles belonging to the resonance region overpredicts the amount of their scattering. Furthermore, during the simulations we saw that increasing scattering caused a decrease of the emissivities. Now, we are able to understand the behaviour in figure 3. The strong decrease of the emissivities with increasing frequencies in the range 10–37 GHz was due to strong scattering on the large air bubbles in the upper ice layers. The strength of this decrease can be controlled by the air bubble radii. Larger particles cause a stronger decrease. In the range above 18.7 GHz, the violation of the Rayleigh approximation leads to an overprediction of scattering and consequently to the discrepancies between theory and experiment. It can be seen from this discussion that by choosing smaller air bubbles and an appropriate ice grain size, a better fit to the observations at 37 GHz and 90 GHz can be achieved. Test calculations have, however, shown that unrealistically small air bubbles, compared with the reported ones, are needed and that the resulting emissivities at 18.7 GHz especially are too high in comparison with the experiment.

In order to describe correctly larger scatterers, belonging from their size to the resonance rather than to the Rayleigh region, Mie instead of Rayleigh scattering has to be included in calculating their dielectric and radiative properties. Up to now, a rigorous and self-consistent treatment of densely packed Mie scatterers within the framework of a discrete scatterer approach based on the Dyson and Bethe-Salpeter equations does not exist as it is given for Rayleigh particles by the DMRT. First attempts to overcome the restriction to small spheres have been made by, e.g., Ding (1989), Ding and Tsang (1989), and Tsang and Kong (1992). In the first two articles, effective propagation constants for media with moderate size spheres were calculated on the basis of QCA. In the last one, the coherent wave was studied within QCA, and the incoherent scattered wave calculated by use of the distorted Born approximation. Numerical results were given for dry snow in the frequency range from 5 to 95 GHz and mean grain radii between 0.3 and 0.9 mm (Tsang and Kong 1992). Comparisons were made with extinction measurements and good agreement obtained.

The numerical solution of the radiative transfer equation (1) allows investigations concerning the fraction of each layer in the total emissivity. In doing so, only the thermal source of the layer under consideration is taken into account. All other layers are treated as purely scattering and absorbing layers without any thermal sources (i.e. $\bar{B}(T) = 0$). In table 4, an example of these calculations is given. Note that the fractions are approximately the same for each polarization. Investigations for this ice type have been undertaken only up to 18.7 GHz since the model fails beyond this frequency.

In the range 6.7–18.7 GHz, the snow layer provides a negligible contribution to the emissivity. At 6.7 GHz, most of the emissivity comes from the ice bottom due to the lower optical thickness of the uppermost ice layers, relative to the other layers. With increasing frequency, the fractions of the layers below 102 cm decreases since

Table 4. Calculated fractions (in %) of various layers in total emissivity at different frequencies and an observation angle of 50° for the ice at DS-7.

Depth range (cm)	6.7 GHz	10 GHz	18.7 GHz
0–46	4	7	26
46–102	37	56	68
102–160	48	35	6
160–∞	11	2	0

the optical thickness of the layers above increases. At 18.7 GHz and higher frequencies, the emissivity contributions of the uppermost ice layers containing relatively large air inclusions become important. At the same time the Rayleigh approximation for these air bubbles is violated leading to the discrepancies between theory and experiment as discussed above.

Figure 4 shows the emissivities as functions of the observation angle at a frequency of 18.7 GHz. The calculated h-polarized emissivities fit the observations very well whereas the v-polarized ones are higher in comparison with the experiment. Figure 3 already indicates this behaviour. Improvements for the v-polarized emissivities can be achieved by varying the air bubble radii, but at the expense of the h-polarized emissivities.

3.3. *Refrozen Del Norte melt pond*

In the next example, the refrozen Del Norte melt pond, Arctic Ocean, north of the Barents Sea, some tens of metres away from DS-7, is considered. Again, experimental data for this site were acquired from 3 October to 8 October 1988, as part

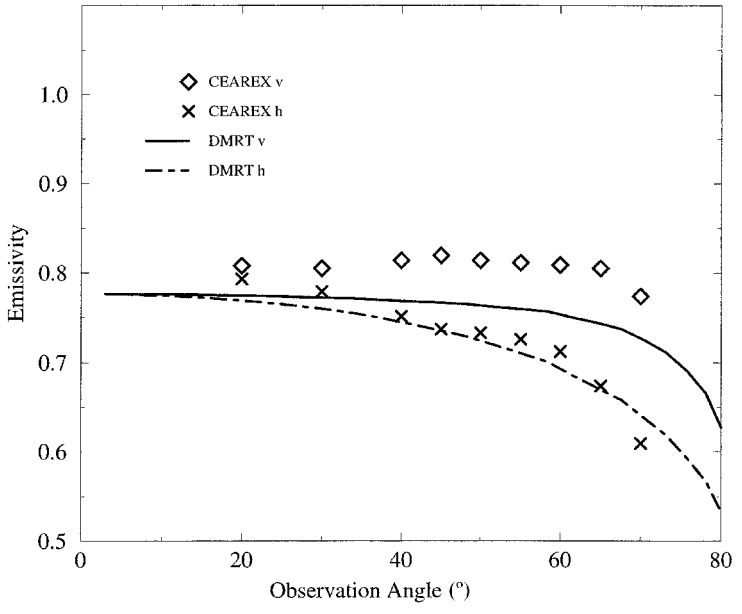

Figure 4. Comparison of observations made during the CEAREX experiment with emissivities computed using the DMRT for the ice at DS-7. Emissivity versus observation angle at 18.7 GHz. The parameters for the DMRT calculations are given in table 3.

of the CEAREX experiment. Details about these data and computational results from different models are given in Winebrenner *et al.* (1992a). The DMRT was also applied to this ice for calculating the 10 GHz backscattering. The like-polarized model results agree with the corresponding observations for angles between 25° and 55° whereas the cross-polarized predictions are too low compared with the experiment.

The ice of the Del Norte melt pond is clear and nearly bubble-free except for the upper 12 cm which is slightly bubbly. The 2 cm thick ice layer with a mean bubble diameter of 1.3 mm reported by Onstott (Winebrenner *et al.* 1992a) was neglected in our computations. In this way, the best fit to the experiment was obtained. Table 5 summarizes the parameters we used. The density and salinity profile were taken from figures 8–13 in Winebrenner *et al.* (1992a). The temperature profile was estimated on the basis of Grenfell's measurements. As for DS-7, the ice grain radius a_{ice} and the brine pocket radius a_{brine} were assumed to be 0.1 mm. We chose small air bubble radii of 0.05 mm according to the mode bubble diameter used in the 10 GHz backscattering calculations by means of the DMRT mentioned above.

Figure 5 provides a comparison between the computational results and measurements for different frequencies at an observation angle of 50°. The agreement for the v-polarization is good except at 10 GHz where a minimum in the experimental data occurs. As for grey ice, we were not able to reproduce this minimum. Another similarity to grey ice is that the h-polarized emissivities at frequencies above 10 GHz lie below the observations (compare with figure 1).

In figure 6, calculated and measured emissivities versus observation angle at 18.7 GHz are plotted. The agreement is quite good for angles ranging from 20° to 60°. An increase of the measured h-polarized values above 60° can be observed so that theory and experiment increasingly disagree. However, the origin of this increase is not clear and could not be observed for grey ice and ice at DS-7.

Table 5. Parameters used in the emissivity calculations for the refrozen Del Norte melt pond. By taking equation (8), the computed ice volume fraction of the snow layer is 0.109. Both air volume fractions for the first two ice layers, calculated by means of the model of Cox and Weeks (1983), are 0.047. Equation (9) provides for the brine volume fractions 5.5×10^{-4}, 1.2×10^{-3}, 3.6×10^{-3}, 5.5×10^{-3}, 6.9×10^{-3}, 5.8×10^{-3}, 7.9×10^{-3}, 8.8×10^{-3}, 8.4×10^{-3}, 9.6×10^{-3} and 9.7×10^{-3}, beginning with the first ice layer.

Medium	d (cm)	T (K)	ρ (g cm^{-3})	S (‰)	a_{ice} (mm)	a_{air} (mm)	a_{brine} (mm)
dry snow	8	259.1	0.1	0	0.1	0	0
sea ice	5	262.3	0.875	0.1	0	0.05	0.1
sea ice	8	263.5	0.875	0.2	0	0.05	0.1
sea ice	15	263.7	0.87	0.6	0	0	0.1
sea ice	6	264.1	0.92	0.9	0	0	0.1
sea ice	10	264.5	0.92	1.1	0	0	0.1
sea ice	10	264.8	0.9	0.9	0	0	0.1
sea ice	10	265.1	0.91	1.2	0	0	0.1
sea ice	9	265.4	0.89	1.3	0	0	0.1
sea ice	13	265.7	0.89	1.2	0	0	0.1
sea ice	11	266.1	0.89	1.3	0	0	0.1
sea ice	53	266.8	0.89	1.2	0	0	0.1
sea water	∞	269.9	1.0	32.0	0	0	0

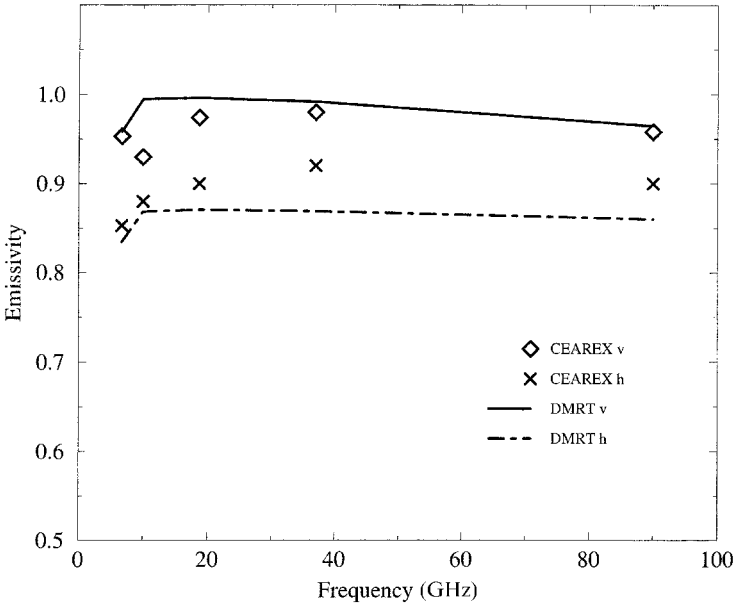

Figure 5. Comparison of observations made during the CEAREX experiment with emissivities computed using the DMRT for the refrozen Del Norte melt pond. Emissivity versus frequency at an observation angle of 50°. The parameters for the DMRT calculations are given in table 5.

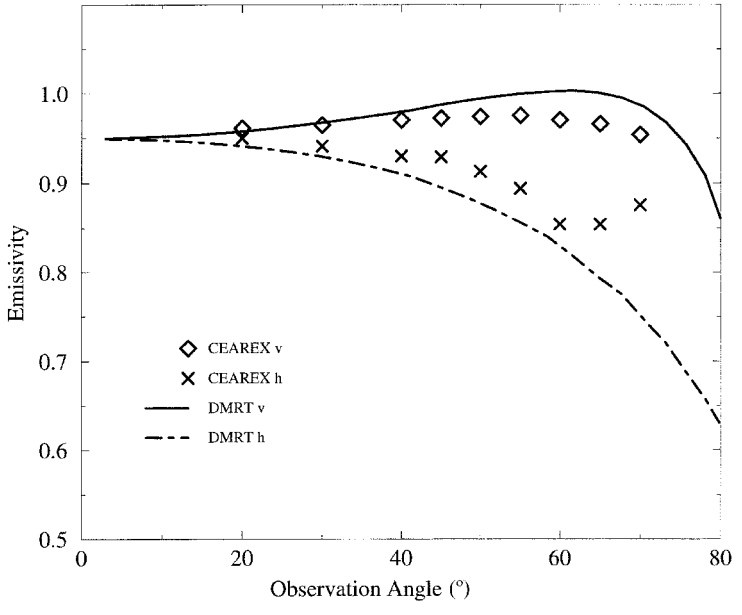

Figure 6. Comparison of observations made during the CEAREX experiment with emissivities computed using the DMRT for the refrozen Del Norte melt pond. Emissivity versus observation angle at 18.7 GHz. The parameters for the DMRT calculations are given in table 5.

3.4. *First-year ice in the Weddell Sea*

The last case study is devoted to first-year ice of the Weddell Sea, Antarctic (Grenfell *et al.* 1994). The data reported there were gained during the cruises V/2 and V/3 of the FS *Polarstern* in the Weddell Sea from July to December 1986 at different ice station sites, within the framework of the Winter Weddell Sea Project (WWSP). However, these data (physical ice properties and emissivities) represent average values from different sites and times. This will make modelling difficult although Grenfell *et al.* (1994) concluded that the average emissivity was relatively constant throughout the experiment. Nevertheless, this ice type was included in our investigations since it provides an example of ice in the Antarctic.

Table 6 shows the parameters we used to model first-year ice of the Weddell Sea. The temperature, density and salinity profiles as well as the liquid water content and ice grain size in snow were taken from figure 5 of Grenfell *et al.* (1994). Furthermore, a constant water bubble radius a_{water} of 0.2 mm was assumed. As in the preceding examples, a brine pocket radius of 0.1 mm was taken for simplicity. In order to model scattering on air bubbles in the ice, an effective scattering layer with $a_{\mathrm{air}} = 0.3$ mm was introduced. Corresponding results for the emissivities are given in figures 7 and 8. The agreement between theory and experiment is acceptable for the h-polarization in the frequency range 10–90 GHz and for the v-polarization in the range 18.7–90 GHz (figure 7). However, the increase of the observed emissivities from 6.7–18.7 GHz was not reproduced by the DMRT. Parameter variations such as changing all bubble radii, changing the thickness of the layer containing the air bubbles or adding air bubbles to other ice layers led to no improvements. This is also the case if the temperature and salinity profiles are modified, if the wet snow is replaced by dry one, or even if the snow cover is totally omitted. We, therefore, conclude that the discrepancies shown in figures 7 and 8 are due to the averaging procedure in obtaining the physical ice parameters and emissivities. Moreover, the periods in which the emissivity and physical data were acquired were different. For instance, the mean ice properties (figure 5 in Grenfell *et al.* (1994)) were gained from July to November 1986. The measurements given in figure 7 were made during the cruise V/2 from July to September 1986, and those in figure 8 were made during

Table 6. Parameters used in the emissivity calculations for first-year ice of the Weddell Sea. Based on equation (8), both ice volume fractions of the snow layers are 0.371. The model of Cox and Weeks (1983) yields an air volume fraction of 0.028 in the first ice layer. By taking equation (9), the computed brine volume fractions are 0.112 for the first ice layer, and 0.120, 0.140, 0.137, 0.145 and 0.157 for the following ice layers.

Medium	d (cm)	T (K)	ρ (g cm^{-3})	S (‰)	f_{water}	a_{ice} (mm)	a_{water} (mm)	a_{air} (mm)	a_{brine} (mm)
wet snow	4	264.0	0.34	8.0	0.05	0.6	0.2	0	0
wet snow	5	265.0	0.34	15.0	0.11	0.7	0.2	0	0
sea ice	10	267.0	0.91	13.5	0	0	0	0.3	0.1
sea ice	10	269.0	0.91	10.0	0	0	0	0	0.1
sea ice	10	270.0	0.91	9.0	0	0	0	0	0.1
sea ice	10	270.5	0.91	7.5	0	0	0	0	0.1
sea ice	10	271.0	0.91	6.5	0	0	0	0	0.1
sea ice	10	271.5	0.91	5.5	0	0	0	0	0.1
sea water	∞	271.5	1.0	32.0	0	0	0	0	0

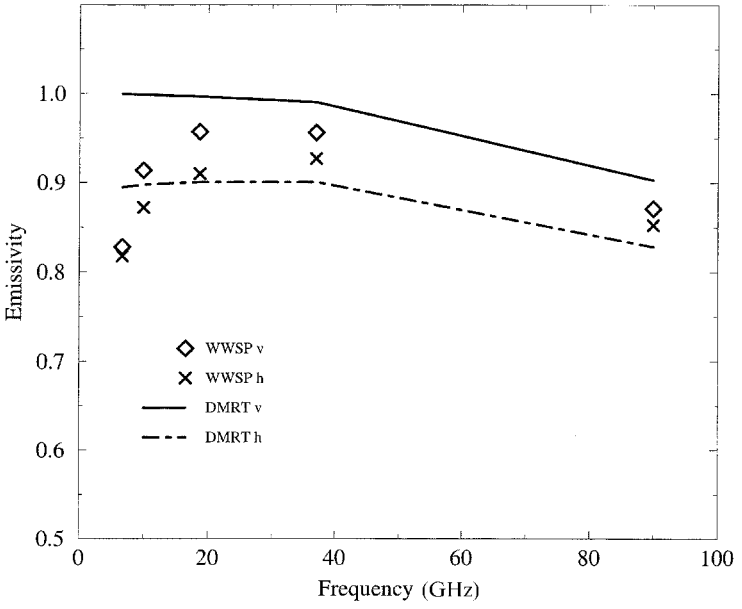

Figure 7. Comparison of observations made during the Winter Weddell Sea Project (WWSP; cruise V/2 from July to September 1986) with emissivities computed using the DMRT for first-year ice of the Weddell Sea. Emissivity versus frequency at an observation angle of 50°. The parameters for the DMRT calculations are given in table 6.

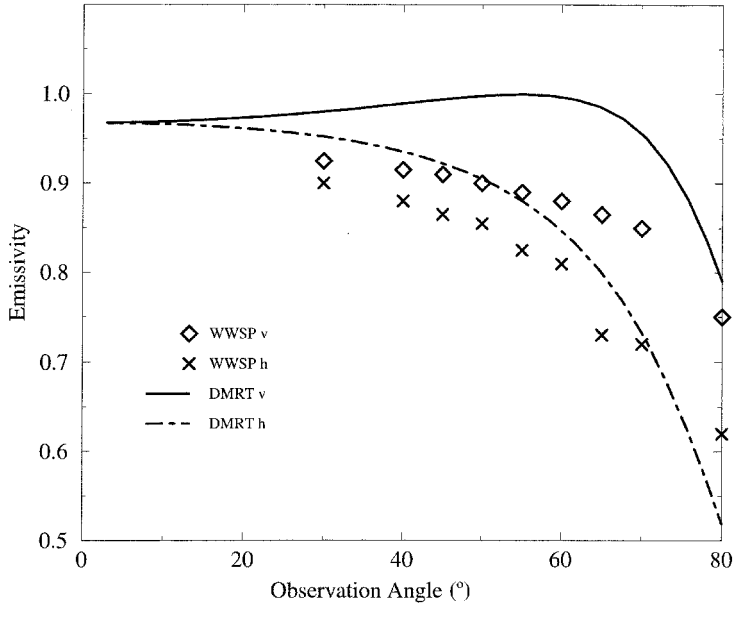

Figure 8. Comparison of observations made during the Winter Weddell Sea Project (WWSP; cruises V/2 and V/3 from July to December 1986) with emissivities computed using the DMRT for first-year ice of the Weddell Sea. Emissivity versus observation angle at 10 GHz. The parameters for the DMRT calculations are given in table 6.

both cruises, V/2 and V/3. Thus, possible changes of the ice with time would lead to additional errors.

The dominant role of the upper two wet snow layers for the total emissivity can be seen in table 7. In the frequency range of 18.7–90 GHz, the snow provides the total emissivity and absorbs practically all radiation coming from the underlying ice and sea water. This behaviour is due to the wetness and salinity of the snow, and is in contrast to that of dry snow present at DS-7 (see §3.2 and table 4) and Del Norte melt pond. In the latter case, the fraction of the dry snow layer in the total emissivity reaches its maximum at 90 GHz with about 9% for each polarization.

Finally, let us consider the size parameters at 90 GHz. For $a_{ice} = 0.7$ mm and 0.6 mm, we have about 1.3 and 1.1, respectively, and for $a_{air} = 0.3$ mm, the size parameter is about 1. In contrast to the situation at DS-7 where essentially larger size parameters occurred, these values should give reasonable emissivities at this frequency. It is not expected that the emissivities alter drastically by using Mie instead of Rayleigh scattering. Note that an ice grain size parameter in snow at 85 GHz of about 1 occurred in calculating brightness temperatures by means of the DMRT in Jin (1997a). It was found in these investigations that equation (6) with $L = 1$, although valid only in the low-frequency limit, yields almost exactly the same results for $k_{bg} \cdot a_{ice} = 0.5$ and 1.0 as in Tsang *et al.* (1985), where numerically calculated K_{eff} for size parameters ranging from 0.05 to 2.5 are given.

4. Conclusions

The results obtained above for thin grey ice, multi-year ice in the Arctic and first-year ice in the Antarctic show that the DMRT is applicable to describe the emission of different sea ice types with or without snow cover. Most of the parameters needed in using the DMRT are determined by proved models based on measurements. In this way, the number of free parameters which can be taken to fit DMRT calculations to experimental observations is limited. In our simulations, these free parameters were given by the size of the scatterers and by the liquid water content of wet snow, if present. We showed that a variety of the experimental results could be explained by choosing realistic particle dimensions reported in the literature. In the case of first-year ice where wet snow occurred, the liquid water content was directly taken from measurements. Since realistic assumptions about the physical ice properties seem to yield reasonable emissivities, the DMRT can, consequently, be used for passive microwave remote sensing of sea ice. This has already been done for snow (e.g. Tsang *et al.* 1992, Chang and Tsang 1992).

Good agreement between theory and experiment could be achieved in the case of relatively homogeneous and weakly scattering ice (grey ice, refrozen Del Norte melt pond) for the v-polarized emissivities versus frequency at an observation angle

Table 7. Calculated fractions (in %) of various layers in the total emissivity at different frequencies and an observation angle of 50° for first-year ice of the Weddell Sea.

Depth range (cm)	6.7 GHz	10 GHz	18.7 GHz	37 GHz	90 GHz
0–4	14	27	64	95	100
4–9	45	57	36	5	0
9–19	36	15	0	0	0
19–29	4	1	0	0	0
29–39	1	0	0	0	0

of 50° and for the emissivities versus observation angle at 18.7 GHz. In contrast to this, the h-polarized emissivities versus frequency were, in general, underpredicted. The reason for this behaviour is not clear. However, simulations done for grey and first-year ice indicate that the h-polarized emissivities as functions of the frequency are very sensitive to the presence of a snow cover. If a snow cover is present, the DMRT results lie above those obtained in the absence of snow. Measurements of the differences between v- and h-polarized emissivities at various frequencies could therefore be useful for remote sensing of snow on sea ice.

In the case of rather inhomogeneous and strongly scattering ice (DS-7), the agreement between theory and observations for both polarizations is good at lower frequencies up to 18.7 GHz. Disagreements arise at higher frequencies due to the violation of the Rayleigh approximation. Additional theoretical work has to be done to extend the DMRT to Mie scattering. For first-year ice in the Weddell Sea, difficulties in comparing computational and experimental results seem to be based on site and time averaging procedures in the reported observations. However, it can be concluded from the calculations that the DMRT is also able to describe this ice type.

The strongest input parameter sensitivities in this model are to the bubble size. Only single-sized spheres have been considered for the different scatterer types in a given layer. It is readily possible to take size distributions into account. However, we have not done this in order to keep the model as simple as possible and to avoid additional free parameters characterizing the size distribution. Furthermore, all computed results were obtained on the basis of the spherical particle assumption. Evidence to consider non-spherical scattering effects was not found. In contrast to this, a variety of other sea ice models assume spheroidal brine pockets (Winebrenner *et al.* 1992a) as observations indicate (Perovich and Gow 1996). The inclusion of such particle shapes into the DMRT requires great theoretical and numerical efforts concerning the description of the single scattering process and the corresponding pair distribution functions.

Acknowledgment

We thank the two anonymous referees for their valuable comments. This work was supported by the Bundesministerium für Bildung, Wissenschaft, Forschung und Technologie (BMBF) under the project number 03PL018C.

References

Carsey, F. D., 1992a, Remote sensing of ice and snow: review and status. *International Journal of Remote Sensing*, **13**, 5–11.

Carsey, F. D. (editor), 1992b, *Microwave Remote Sensing of Sea Ice*, Geophysical Monograph 68 (Washington: American Geophysical Union).

Chandrasekhar, S., 1960, *Radiative Transfer* (New York: Dover Publications).

Chang, A. T. C., and Tsang, L., 1992, A neural network approach to inversion of snow water equivalent from passive microwave measurements. *Nordic Hydrology*, **23**, 173–182.

Cox, G. F. N., and Weeks, W. F., 1983, Equations for determining the gas and brine volumes in sea-ice samples. *Journal of Glaciology*, **29**, 306–316.

Dierking, W., 1992, Sensitivity studies of selected theoretical scattering models with applications to radar remote sensing of sea ice. AWI Berichte aus dem Fachbereich Physik, Report 33, Alfred-Wegener-Institut für Polar und Meeresforschung, Bremerhaven, Germany.

Ding, K. H., 1989, Electromagnetic wave propagation and scattering in dense media. PhD thesis, University of Washington, Seattle, USA.

Ding, K. H., Mandt, C. E., Tsang, L., and Kong, J. A., 1992, Monte Carlo simulations of pair distribution functions of dense discrete random media with multiple sizes of particles. *Journal of Electromagnetic Waves and Applications*, **6**, 1015–1029.

Ding, K. H., and Tsang, L., 1988, Effective propagation constants of dense nontenuous media with multi-species of particles. *Journal of Electromagnetic Waves and Applications*, **2**, 757–777.

Ding, K. H., and Tsang, L., 1989, Effective propagation constants in media with densely distributed dielectric particles of multiple sizes and permittivities. In *Progress in Electromagnetics Research* PIER 1, edited by J. A. Kong (New York: Elsevier), pp. 241–295.

Ding, K. H., Yang, Y. E., Shih, S. E., Kong, J. A., and Davis, R. E., 1996, Modelling of electromagnetic wave scattering from time-varying snow-cover. Remote sensing for a sustainable future. Vol. 1. *Proceedings of the International Geoscience and Remote Sensing Symposium IGARSS'96, Lincoln, NE, USA, 27–31 May 1996* (New York: Institute of Electrical and Electronics Engineers), pp. 757–759.

Fung, A. K., 1994, *Microwave Scattering and Emission Models and Their Applications* (Boston: Artech House).

Grenfell, C., Comiso, J. C., Lange, M. A., Eicken, H., and Wensnahan, M. R., 1994, Passive microwave observations of the Weddell Sea during austral winter and early spring. *Journal of Geophysical Research*, **99**, 9995–10010.

Jin, Y.-Q., 1993, *Electromagnetic Scattering Modelling for Quantitative Remote Sensing* (Singapore: World Scientific).

Jin, Y.-Q., 1997a, Simulation of a multi-layer model of dense scatterers for anomalous scattering signatures from SSM/I snow data. *International Journal of Remote Sensing*, **18**, 2531–2538.

Jin, Y.-Q., 1997b, Radiative transfer of snowpack/vegetation canopy at the SSM/I channels and satellite data analysis. *Remote Sensing of Environment*, **61**, 55–63.

Klein, L. A., and Swift, C. T., 1977, An improved model for the dielectric constant of sea water at microwave frequencies. *IEEE Transactions on Antennas and Propagation*, **AP-25**, 104–111.

Mätzler, C., and Wegmüller, U., 1987, Dielectric properties of freshwater ice at microwave frequencies. *Journal of Physics D: Applied Physics*, **20**, 1623–1630; 1988, Erratum. *Journal of Physics D: Applied Physics*, **21**, 1660.

Perovich, D. K., and Gow, A. J., 1996, A quantitative description of sea ice inclusions. *Journal of Geophysical Research C*, **101**, 18327–18343.

Poe, G., Stogryn, A., and Edgerton, A. T., 1972, A study of the microwave emission characteristics of sea ice. Final Technical Report 1749R-2, Contract No. 2-35340, Aerojet Electrosystems Co., Azusa, California, USA.

Stamnes, K., Tsay, S.-C., Wiscombe, W., and Jayaweera, K., 1988, Numerically stable algorithm for discrete-ordinate-method radiative transfer in multiple scattering and emitting layered media. *Applied Optics*, **27**, 2502–2509.

Stogryn, A., and Desargant, G. J., 1985, The dielectric properties of brine in sea ice at microwave frequencies. *IEEE Transactions on Antennas and Propagation*, **AP-33**, 523–532.

Tsang, L., 1987, Passive remote sensing of dense nontenuous media. *Journal of Electromagnetic Waves and Applications*, **1**, 159–173.

Tsang, L., 1992, Dense media radiative transfer theory for dense discrete random media with particles of multiple sizes and permittivities. In *Dielectric Properties of Heterogeneous Materials*, PIER 6, edited by A. Priou (New York: Elsevier), pp. 181–230.

Tsang, L., Chen, Z., Oh, S., Marks II, R. J., and Chang, A. T. C., 1992, Inversion of snow parameters from passive microwave remote sensing measurements by a neural network trained with a multiple scattering model. *IEEE Transactions on Geoscience and Remote Sensing*, **30**, 1015–1024.

Tsang, L., Ding, K. H., and Wen, B., 1990, Polarimetric signature of random discrete scatterers based on vector radiative transfer theory. In *Polarimetric Remote Sensing*, PIER 3, edited by J. A. Kong (New York: Elsevier), pp. 75–142.

TSANG, L., and ISHIMARU, A., 1987, Radiative wave equations for vector electromagnetic propagation in dense nontenuous media. *Journal of Electromagnetic Waves and Applications*, **1**, 59–72.

TSANG, L., and KONG, J. A., 1992, Scattering of electromagnetic waves from a dense medium consisting of correlated Mie scatterers with size distributions and applications to dry snow. *Journal of Electromagnetic Waves and Applications*, **6**, 265–286.

TSANG, L., KONG, J. A., and SHIN, R. T., 1985, *Theory of Microwave Remote Sensing* (New York: John Wiley & Sons).

ULABY, F. T., MOORE, R. K., and FUNG, A. K., 1986, *Microwave Remote Sensing: Active and Passive, Volume III: From Theory to Applications* (Norwood: Artech House).

WEN, B., TSANG, L., WINEBRENNER, D. P., and ISHIMARU, A., 1990, Dense medium radiative transfer theory: comparison with experiment and application to microwave remote sensing and polarimetry. *IEEE Transactions on Geoscience and Remote Sensing*, **28**, 46–59.

WEST, R. D., TSANG, L., and WINEBRENNER, D. P., 1993, Dense medium radiative transfer theory for two scattering layers with a Rayleigh distribution of particle sizes. *IEEE Transactions on Geoscience and Remote Sensing*, **31**, 426–437.

WEST, R. D., WINEBRENNER, D. P., and TSANG, L., 1994, The influence of layering and grain size on microwave emission from polar firn. *Proceedings of the International Geoscience and Remote Sensing Symposium IGARSS'94, Pasadena, California, USA, 8–12 August 1994* (Piscataway, NJ: Institute of Electrical and Electronics Engineers), paper number 940260.

WINEBRENNER, D. P., BREDOW, J., FUNG, A. K., DRINKWATER, M. R., NGHIEM, S., GOW, A. J., PEROVICH, D. K., GRENFELL, T. C., HAN, H. C., KONG, J. A., LEE, J. K., MUDALIAR, S., ONSTOTT, R. G., TSANG, L., and WEST, R. D., 1992a, Microwave sea ice signature modeling. In *Microwave Remote Sensing of Sea Ice*, Geophysical Monograph 68, edited by F. D. Carsey (Washington: American Geophysical Union), pp. 137–175.

WINEBRENNER, D. P., JOUGHIN, I. R., and FAHNESTOCK, M. A., 1997, Interferometric SAR for observation of glacier motion and firn penetration. *Proceedings of the 3rd ERS Scientific Symposium, Florence, Italy, 17–21 March 1997*, vol. 2, SP-414 (Paris: European Space Agency).

WINEBRENNER, D. P., TSANG, L., WEN, B., and WEST, R. D., 1989, Sea-ice characterization measurements needed for testing of microwave remote sensing models. *IEEE Journal of Oceanic Engineering*, **14**, 149–158.

WINEBRENNER, D. P., TSANG, L., WEN, B., and WEST, R. D., 1992b, Sensitivities for two polarimetric backscattering models for sea ice to geophysical parameters. In *Direct and Inverse Methods in Radar Polarimetry*, Part 2, edited by W. M. Boerner *et al.* (Dordrecht: Kluwer Academic Publishers), pp. 1191–1212.